An Imaging and Spectroscopic Study of RCW 103

Authors: C. Braun, S. Safi-Harb (University of Manitoba); C. Fryer (Los Alamos National Laboratory)

Motivation

RCW 103 is an SNR hosting a peculiar CCO 1E 161348-5055 that displays strong X-ray variability and a periodicity of 6.67 hr (De Luca et al. 2006). Recently, the CCO went into a period of bursting activity (e.g., Rea et al. 2016) and the 6.67 h periodicity has been interpreted as the rotation period of the slowest know magnetar to date. Although plenty of studies have examined the CCO, little has been done on the remnant itself.

This work is part of a more global study of SNRs, to be presented in follow-up studies, using X-ray imaging and spectroscopy aimed at addressing the SN progenitors and explosion properties of SNRs hosting CCOs (Safi-Harb, 2017). Our study is additionally motivated by performing a systematic study using the latest nucleosynthesis models available to the SNR community, while also providing feedback to modellers given the current limitation and assumptions made on nucleosynthesis yields.

Data Analysis

This study used archival data from *Chandra* and *XMM-Newton:*

ObsID	Detector	Effective Exposure time (ks)	Observation date (DD/MM/YY)
123	ACIS-I	13.36	26/06/99
970	ACIS-S	17.46	08/08/00
11823	ACIS-I	62.47	01/06/10
12224	ACIS-I	17.82	27/06/10
17460	ACIS-I	24.76	13/01/15
0113050601	MOS 1/2	16.0/15.2	03/09/01
0113050701	MOS 1/2	12.4/9.4	03/09/01
0302390101	MOS 1/2	60.2/55.0	23/08/05

Table 1: Data sets used in the study.

Imaging:

A *Chandra* RGB image using all datasets can be seen in Figure 1 (top left). Defining features are the lobed structure, the hard X-ray CCO point source, and the ``C-shaped'' hole north-east of the CCO.

XMM-Newton continuum subtracted line images for Fe L, Mg, Si, and S and using all data sets are displayed in Figure 1 (middle & bottom left). The morphology in our line images show they follow the overall lobed structure as seen in the RGB image.

Spectroscopy:

54 regions from *Chandra* data were extracted for the spectroscopic study (Figure 2). Most regions were well fit by two-component VPSHOCK+APEC models, in contrast to Frank et al. (2015) who used one-component models. The hard component is overall associated with the VPSHOCK model, and had variable temperature, abundances (Mg, Si, S, and Fe (Ni)), and ionization timescale. The soft component is associated with the APEC model and has variable temperature (0.2–0.5 keV), abundances consistent with solar, and has reached ionization equilibrium.

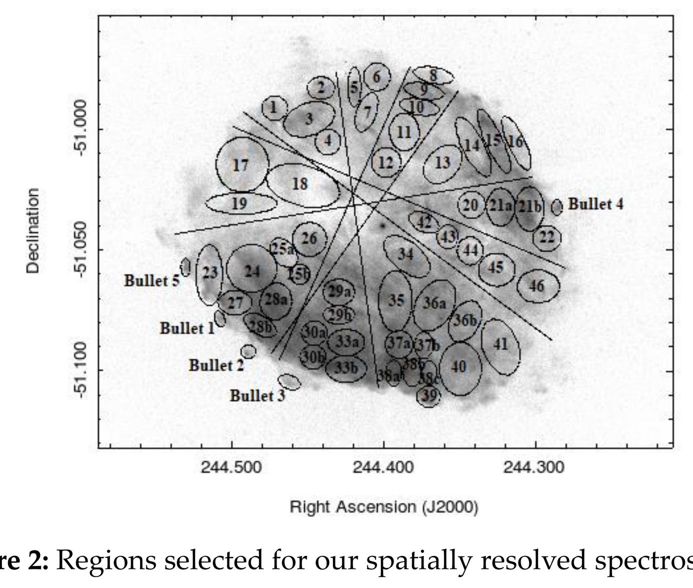

Figure 2: Regions selected for our spatially resolved spectroscopy.

Results

Values for the full SNR fit are displayed in Table 2 and these would represent representative averaged values for the regions in Figure 2.

Full SNR fit: VPSHOCK+APEC	
n_H ($\times 10^{22}$ cm^{-2})	1.05
Hard VPSHOCK	
kT (keV)	0.56
Mg	1.3
Si	1.4
S	1.0
Fe = Ni	1.2
$n_e t$ ($\times 10^{11}$ cm^{-3} s)	16.1
Soft APEC	
kT (keV)	0.19

Table 2: Full SNR VPSHOCK+APEC model best fit.

The shocked heated ejecta are associated with the hard component, with temperature kT ≈ 0.6 keV, slightly enhanced abundance yields, and still in non-equilibrium ionization with values $n_e t \approx 10^{11}$–10^{12} cm^{-3} s. The blast wave component is associated with the soft component showing abundances consistent with solar, with a temperature kT ≈ 0.2 keV, and has reached ionization equilibrium. However, there are single-component regions with subsolar abundances and higher temperatures that may indicate there is a range of temperature values for the blast wave component.

A progenitor study was performed using the newest models: bipolar explosion models (Maeda & Nomoto 2003), hypernova models (Nomoto et al. 2006), a suite of spherical explosions using a range of progenitor masses (Sukhbold et al. 2016), and a recent set of explosion models using 3 progenitors but with a broad range of explosions (Fryer et al. 2018). Degeneracies in the model fitting were also explored. Best fit progenitor models are seen in Figure 1 (right, top and bottom).

Conclusion

RCW 103 was sectioned into 54 regions spanning the entire SNR. The regions were best fit by a two-component VPSHOCK+APEC model where the shock heated ejecta was associated with the hard (0.6 keV) component, with slightly enhanced abundances, and still in non-equilibrium ionization and the blast wave associated with the soft component (0.2 keV), solar abundances, and indicating it has reached ionization equilibrium.

Quantitative Results	
Distance (kpc)	4.7 (3.3−6.3)
M_{SW} ($f_s^{-1/2} D_{3.1}^{5/2}$ $M_\odot$)	16
V_S (km s^{-1}; Sedov)	400
Age ($D_{3.1}$ kyr)	0.88−4.4
n_0 ($f_s^{-1/2} D_{3.1}^{-1/2}$ cm^{-3})	1.2
E_* ($f_s^{-1/2} D_{3.1}^{5/2}$ erg)	3.7×10^{49}
Progenitor Mass ($M_\odot$)	12−13

Table 3: Quantitative results from the study for the distance, swept-up mass (M_{SW}), shock velocity (V_S), age, ambient density (n_0), explosion energy (E_*), and progenitor mass.

A low explosion energy was calculated as 3.7×10^{49} $f_s^{-1/2} D_{3.1}^{5/2}$ erg assuming a Sedov blast wave model, but if we consider the SNR is expanding into the wind bubble of its progenitor, we get an explosion energy of 1.2×10^{50} $f_s^{-1/2} D_{3.1}^{5/2}$ erg. The explosion energy inferred from our X-ray spectroscopy is low ($<2.0\times10^{50}$ $f_s^{-1/2} D_{3.1}^{5/2}$ erg) in comparison to standard explosion energies assumed for supernovae, regardless of the assumptions made on the evolutionary stage, ambient environment, and exact blast wave temperature.

From the progenitor studies the standard explosion models did not match the ejecta yields for RCW 103. The best estimate gives a progenitor mass of 12−13 $M_\odot$. It is likely that a good fit can be found for lower mass progenitors with the right explosion energy. A magnetized CCO could possibly re-eject fallback material, allowing lower explosion energies to still match the observed abundances.

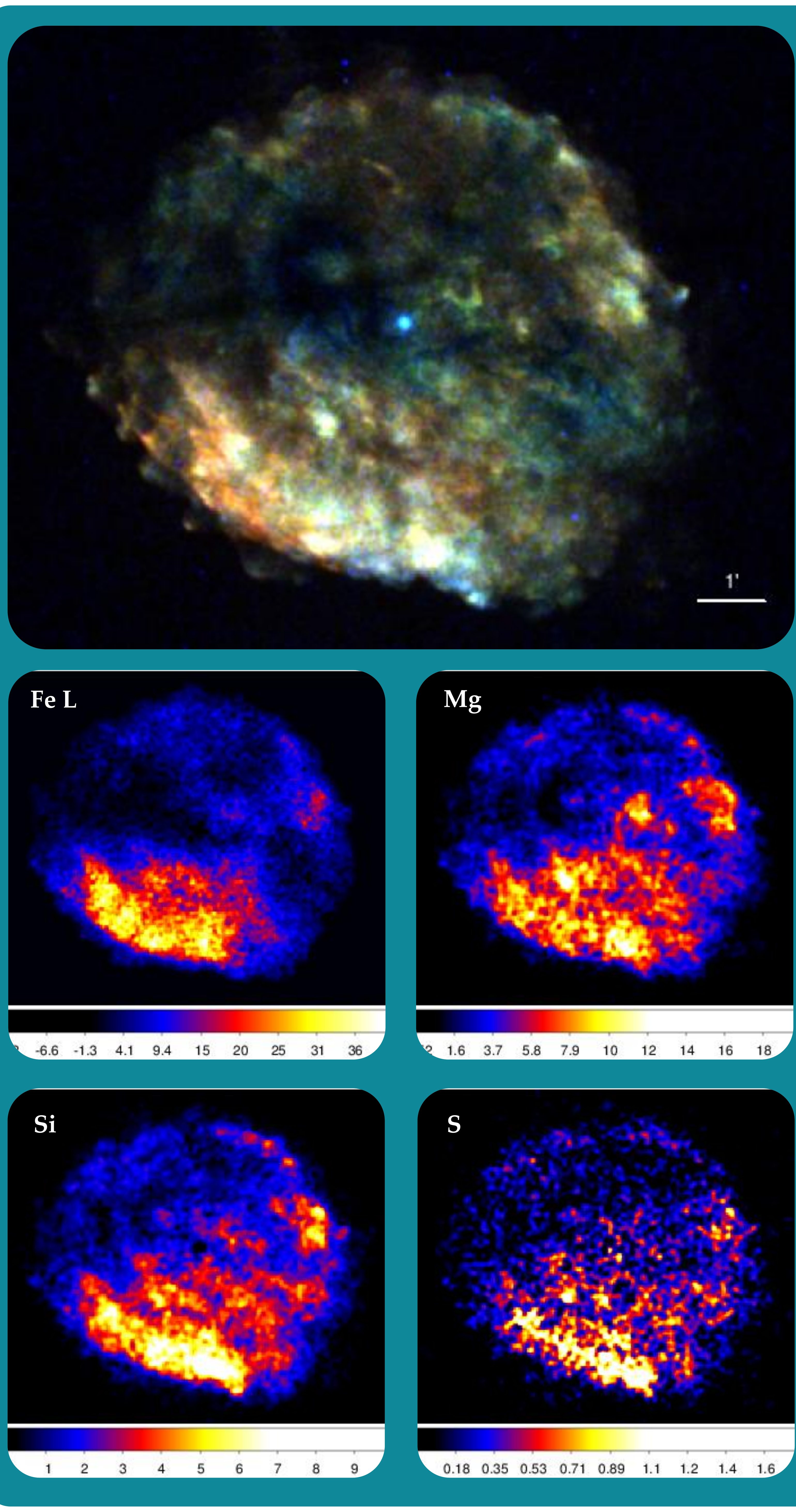

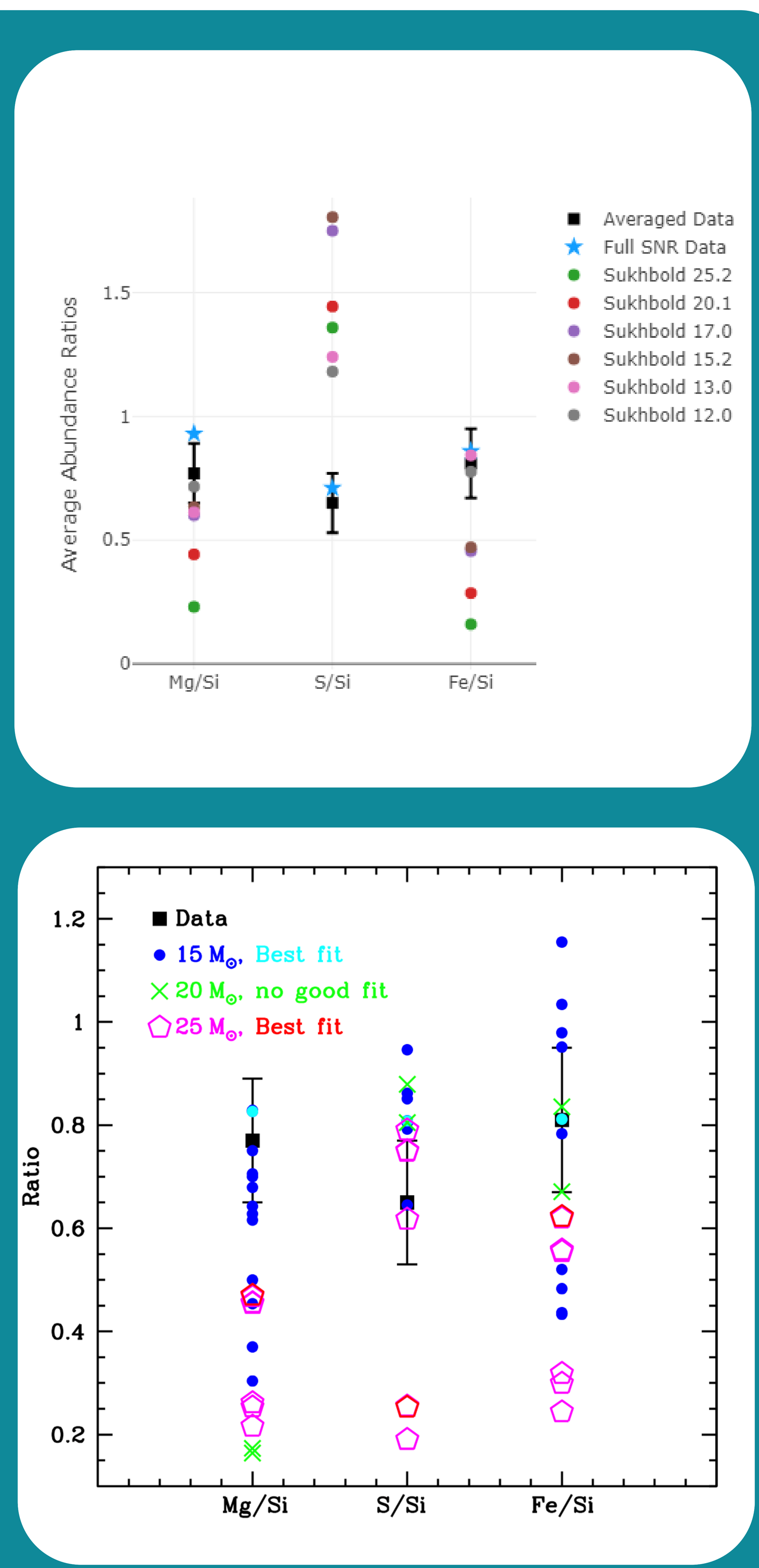

Figure 1:

(Top Left) A *Chandra* RGB image of RCW 103 using all available data sets. The red, green, and blue colours correspond to energy ranges 0.5–1.2 keV, 1.2–2.0 keV, and 2.0–7.0 keV respectively. The image has been smoothed using a Gaussian with radius 3 pixels. North is up and east is left. The remnant is roughly 10´´ in diameter and has a clear bilateral structure with prominent lobes in the northwest and south. Other prominent features are the ``C-shaped'' hole and the bright, hard CCO in the center.

(Middle and Bottom Left) *XMM-Newton* continuum subtracted line images using all available data sets for Fe L, Mg, Si and S each smoothed using a Gaussian with a radius of 2 pixels. These images follow the over-all lobed structure as seen in the RGB image.

(Top Right) Best-fit abundances for Mg, S, and Fe relative to Si relative to solar values for the averaged abundance values from all 54 regions using a room mean-square for the error bars (black) and the star indicating the abundance yields from the full SNR fit. Over-plotted are the predicted relative abundances from the core-collapse nucleosynthesis models from Sukhbold (2016).

(Bottom Right) Similarly to the top right figure, but for varying masses and progenitor explosion energies from Fryer (2018). The blue circles correspond to 15 $M_\odot$ progenitor explosions (cyan producing the best fit statistically), the crosses correspond to 20 $M_\odot$ progenitor explosions (no good fits) and the magenta pentagons correspond to 25 $M_\odot$ progenitor explosions (the red is the best fit). Similarly to the Sukhbold models, the lowest-mass models fits the data better.

Citations:
De Luca A., Caraveo P. A., Mereghetti S., Tiengo A., Bignami G. F., 2006, Science, 313, 814
Frank K. A., Burrows D. N., Park S., 2015, ApJ, 810, 113
Fryer C. L., Andrews S., Even W., Heger A., Safi-Harb S., 2018, ApJ, 856, 63
Katsuda S., Tsunemi H., Uchida H., Kimura M., 2008, ApJ, 689, 225
Maeda K., Nomoto K., 2003, ApJ, 598, 1163
Rea N., Borghese A., Esposito P., Coti Zelati F., Bachetti M., Israel G. L., De Luca A., 2016, ApJ, 828, L13
Safi-Harb S., 2017, in Journal of Physics Conference Series. p. 012005 (arXiv:1712.06040), doi:10.1088/1742-6596/932/1/012005
Sukhbold T., Ertl T., Woosley S. E., Brown J. M., Janka H.-T., 2016, ApJ, 821, 38

This work is presented in detail in the following paper:
Braun C., Safi-Harb S., Fryer C. 2019, *submitted for publication*

Contact Me:
Chelsea Braun
University of Manitoba, Winnipeg, MB, CAN
umbrau59@myumanitoba.ca

NSERC CRSNG

University of Manitoba